ELSEVIER

Flow of Newtonian and non-Newtonian fluids in an eccentric annulus with rotation of the inner cylinder

J. M. Nouri and J. H. Whitelaw
Imperial College of Science, Technology and Medicine, Mechanical Engineering Department, Thermofluids Section, London, UK

Three velocity components of a Newtonian and a weakly elastic shear-thinning non-Newtonian fluid have been measured in an annulus with an eccentricity of 0.5, a diameter ratio of 0.5, and an inner cylinder rotation of 300 rpm. The results show that the rotation had similar effects on the Newtonian and non-Newtonian fluids, with a more uniform axial flow across the annulus and the maximum tangential velocities in the narrowest gap in both cases. The secondary flow circulation with the Newtonian fluid at a Reynolds number of 26,600 was in the direction of the rotation, with maximum values of 14% of the bulk velocity close to the inner pipe. With the 0.2% CMC polymer solution in laminar flow, rotation caused a narrow counter-rotating flow along the outer pipe wall, which was absent at a Reynolds number 9200. The turbulence intensities in the region of widest gap were uninfluenced by rotation, increased in the Newtonian fluid, and decreased in the non-Newtonian fluid in the region of the smallest gap. The flow resistance of both fluids increased with rotation at low Reynolds numbers and reduced with increasing values to become similar to those of nonrotating flows. Comparison between rotating results of the Newtonian and non-Newtonian fluids at a Reynolds number 9200 and the same inner cylinder rotation, showed effects similar to those of nonrotating flow with extension of nonturbulent flow, large reduction in turbulence intensities and drag reduction of the order of 61% for the CMC solution. The swirl velocities in both fluids were similar when the Rossby numbers were similar.

Keywords: eccentric annulus; inner cylinder rotation; velocity; Newtonian and shear-thinning fluids

Introduction

The present investigation is concerned with the measurement of pressure and velocity of Newtonian and non-Newtonian fluids in an eccentric annulus with rotation of the inner cylinder and is a continuation of earlier work of Nouri and Whitelaw (1994), where a concentric annulus was considered. It has many applications in industry; for example, in bearings and in the drilling of oil wells. The latter case motivated the present research and, in practice, involves removal of the friction-generated heat, the transport of cuttings to the surface by mud, and knowledge of the pumping pressures and consequent flow rates. The fluids used in drilling are usually non-Newtonian with low effective viscosity and high effective yield stress, in order to transport the cuttings and to keep solids in suspension during stationary periods. In directional drilling, the annulus usually becomes eccentric, which further complicates the flow and, because the velocity is lowest in the narrowest gap, there is a tendency for cuttings to accumulate, and this effect is less with turbulent flow. Thus, knowledge of the flow characteristics in the annulus as a function of Reynolds number, shaft rotation, and flow geometry, together with the variation of viscometric viscosity, are essential. The present results provide some of this knowledge and have been obtained in sufficient detail to allow their use as input boundary conditions and for the appraisal of the results of CFD calculations.

Previous investigations of rotating and nonrotating Newtonian flows in concentric and eccentric annuli have been discussed by Nouri and Whitelaw (1994) and Nouri et al. (1993) and are summarized in Table 1. Experimental investigations of the flow velocity characteristics of non-Newtonian fluids in annuli are limited to those of Nouri and Whitelaw (1994) and Nouri et al. (1993) who used an aqueous solution of sodium carbomethyl cellulose (CMC, a weakly elastic shear-thinning polymer) to model the drilling mud and Escudier et al. (1994), who used three shear-thinning aqueous solutions of CMC, xanthan gum and a laponite/CMC blend, with the last being thixotropic. In the last investigation, the concentric annulus was 2.5 times larger than in the two former studies but with the same diameter ratio, and the agreement between the CMC results was very good, showing a similar flow resistance to that of a Newtonian fluid in the laminar flow regime, with clear evidence of drag reduction in turbulent flow, consistent with the large suppression of cross-flow

Address reprint requests to Prof. J. H. Whitelaw, Dept. of Mechanical Engineering, Imperial College, Exhibition Road, London SW7 2BX, UK.

Received 28 November 1995; accepted 9 June 1996

Int. J. Heat and Fluid Flow 18: 236–246, 1997

655 Avenue of the Americas, New York, NY 10010

0142-727X/97/$17.00
PII S0142-727X(96)00086-4

turbulence intensities. With rotation of the inner cylinder, the only detailed experimental studies in concentric configurations are those reported by Kuzay and Scott (1973) for air flow, and by Nouri and Whitelaw (1994) and Escudier and Gouldson (1995) for Newtonian and non-Newtonian fluids. In general, the swirl velocity decayed rapidly from the rotating inner cylinder with a much smaller decay in most of the core region and the penetration of swirl decreasing with increase in Reynolds number. Rotation also caused a more uniform axial mean flow and increased the flow resistance. The results of Nouri and Whitelaw (1994) also showed that rotation enhanced the overall turbulence intensities, in particular the cross-flow components with both fluids, that the drag reduction effect associated with the shear-thinning non-Newtonian fluid was larger with rotation, as was the difference in turbulence intensities between the Newtonian and non-Newtonian fluids for the same Reynolds number.

There is no experimental study of flow of Newtonian and non-Newtonian fluids in eccentric annuli with inner cylinder rotation, and the present investigation shows the effects of centerbody rotation on the flow structure with both fluids and for different Reynolds numbers. The measurements were obtained with an eccentricity of 0.5, defined by

$$e = \frac{L}{(R_o - R_{\text{in}})} \tag{1}$$

with L the distance between the centers of the inner and outer pipes and R_{in} and R_o the inner and outer radii, and the inner cylinder rotating at 300 rpm. The results are compared with rotating flow in concentric annuli and with nonrotating flow in concentric and eccentric annuli. The Reynolds numbers based on bulk-flow velocity U_b, hydraulic diameter d_h, and fluid viscosity ν for the Newtonian fluids were 9000 and 26,600 and for the 0.2% aqueous solution of CMC 1150 and 9200. The rotational Reynolds number is defined as $\text{Re}_\omega = \omega R_{\text{in}} S_{\text{av}}/\nu$ where ω is the inner cylinder angular velocity and S_{av} the average gap $0.5d_h$ to give overall rotational Reynolds numbers of 1930 for the Newtonian fluid and 336 and 533 for the non-Newtonian fluid. A useful nondimensional parameter to characterize the rotating flows is the ratio of the bulk-flow Reynolds number to that of the rotational Reynolds number

$$\text{Rs} = \frac{2U_b}{\omega R_{\text{in}}} \tag{2}$$

which represents the ratio of inertial to Coriolis forces and is referred to as the Rossby number with values listed in Tables 2 and 3. In the present case, ω is constant so that a variation in Rossby number is due to a change in bulk flow, and a value of unity implies that the effect of rotation is of the same order as the inertia.

The flow configuration and instrumentation are described briefly in the following section, and the results are presented and discussed in the third section. The paper ends with a summary of the more important findings.

Flow configuration and instrumentation

The flow arrangement was similar to that of Nouri and Whitelaw (1994) and is shown in Figure 1, with the details of the plexiglass test section and coordinate system in Figure 1b. A centrifugal pump delivered the working fluid from a supply tank to a chamber, where, after passing through a section of honeycomb and a contraction, it flowed into the annular passage. The bulk mass flow was measured by a calibrated orifice plate with precision better than 3%, and it remained constant with rotation of the inner cylinder, up to 350 rpm, within the measuring uncertainties.

The Newtonian fluid was a mixture of 31.8% tetraline in turpentine and was maintained at a constant temperature of 25 ± 0.02°C to provide a refractive index equal to that of the plexiglass material of the working section (see Nouri et al. 1988 for further details). The non-Newtonian fluid was a 0.2% aqueous solution of CMC with a viscometric power law relating shear stress τ to shear rate γ as

$$\tau = 0.044\gamma^{0.75} \tag{3}$$

where the power law consistency 0.044 Pa·s, and power-law index 0.75 were obtained from the viscometric data of Pinho and Whitelaw (1990). The main reasons for selecting this polymer solution were its low effective viscosity, up to ten times that of

Notation

C_f	skin-friction coefficient $(\partial P/\partial z)[d_h/2\rho U_b^2]$
d_h	hydraulic diameter $(D_o - D_{\text{in}})$, m
d_r	drag reduction $100 \times [(C_{f_n} - C_{f_p})/C_{f_n}]$
e	eccentricity $[L/(R_0 - R_{\text{in}})]$
D_{in}	inner cylinder diameter, m
D_o	outer pipe diameter, m
L	distance between the centers of the inner and outer pipes
r	radial coordinate, m
r_1	radial distance from the outer wall, m
r_2	radial distance from the inner wall, m
∂P	axial wall pressure drop, N/m^2
R_{in}	inner cylinder radius, m
R_o	outer pipe radius, m
Re	bulk flow Reynolds number $U_b d_h/\nu$
Re_ω	rotational Reynolds number $\omega R_{\text{in}} S_{\text{av}}/\nu$
Rs	Rossby number $2U_b/\omega R_{\text{in}}$
Rs_m	local Rossby number $2U_m/\omega R_{\text{in}}$
S	gap between the inner and outer wall, m
S_{av}	average gap between the inner and outer wall, m
$\tilde{u}, \tilde{v}, \tilde{w}$	rms velocity fluctuations in z, r and θ directions, m/s
$\overline{uv}$	Reynolds shear stress, m^2/s^2
$\overline{U}, \overline{V}, \overline{W}$	mean velocity components in z, r, and θ directions, m/s
U_b	bulk velocity, m/s
U_m	maximum axial mean velocity in each gap, m/s
V_t	inner cylinder surface rotational velocity, m/s
z	axial coordinate, m

Greek

γ	shear rate, 1/s
λ	laser light wave length, nm
μ_w	viscosity at the wall for polymer solution, kg/m·s
ν	fluid kinematic viscosity, m^2/s
θ	angular coordinate, degrees
ρ	fluid density, kg/m^3
τ	shear stress, N/m^2
ω	inner cylinder angular velocity, rad/s

water, consistent with previous investigations carried out with the same fluid in ducts by Pinho and Whitelaw (1990, 1991) and mixing vessels by Nouri and Whitelaw (1990), and its transparency, which allowed the use of laser velocimetry for the velocity measurements.

The length upstream of the test section was 2.32 m, corresponding to 116 hydraulic diameters or 58 outer-pipe diameters. The inner cylinder was driven by a dc motor via a bevel gear box located downstream of the test section, as shown in Figure 1(a), and the rotational speed was measured using an optical shaft

Table 1 Previous experimental investigation

Authors	Fluid	Flow configuration	Flow region	Measuring technique and measured quantity
(a) Nonrotating flow				
Brighton and Jones (1964)	Newtonian, air	$e=0.0$ $D_{in}/D_o=0.062$, 0.125, 0.375, and 0.562	Turbulent	—Manometer and forward facing pitot tube and hot-wire anemometer. —Axial pressure drop and two velocity components
Jonsson and Sparrow (1966)	Newtonian, air	$e=0.0$ to 1.0 $D_{in}/D_o=0.281$, 0.561, and 0.75	Turbulent	—Manometer and pitot tube —Axial pressure drop and axial mean velocity
Quarmby (1967)	Newtonian, air	$e=0.0$ $D_{in}/D_o=0.107$, 0.178, and 0.347	Turbulent	—Manometer and pitot tube —Axial pressure drop and axial mean velocity
Lawn and Elliott (1972)	Newtonian, air	$e=0.0$ $D_{in}/D_o=0.088$, 0.176, and 0.396	Turbulent	—Manometer and hot-wire anemometer —Axial pressure drop and axial mean velocity
Kacker (1973)	Newtonian, air	$D_{in}/D_o=0.176$ 1-single inner pipe, $e=0.475$ 2-two inner pipes	Turbulent	—Pressure transducer, pitot tube and hot-wire anemometer —Axial pressure drop, mean axial and secondary flow velocities
Rehme (1974)	Newtonian, air	$e=0.0$ $D_{in}/D_o=0.020$, 0.040, and 0.1	Turbulent	—Manometer, pitot, and Preston tubes and hot-wire anemometer —Axial pressure drop, axial mean velocity, and wall shear stress
Nouri et al. (1993)	Newtonian, glycerol, and 32% tetraline in turpentine non-Newtonian, 0.2% aqueous solution of CMC	$e=0.0$, 0.5 and 1.0 $D_{in}/D_o=0.5$ $D_o=40.3$ mm	Laminar and turbulent	—Manometer, laser-Doppler velocimeter —Axial pressure drop, three components of mean and rms velocities, and Reynolds shear stresses
Escudier et al. (1994)	Newtonian, glucose syrup Non-Newtonian, three aqueous solutions; CMC, xanthan gum and laponite/CMC blend	$e=0.0$ $D_{in}/D_o=0.506$ $D_o=100.4$ mm	Laminar and turbulent	—Pressure transducer, laser-Doppler velocimeter —Axial pressure drop, axial and tangential mean and rms velocities
(b) Rotating flow ($r=1$)				
Yamada (1962)	Newtonian, water	$e=0.0$ $D_{in}/D_o=0.897$, 0.913, 0.955, 0.97, 0.98, and 0.986 Inner pipe rotating from 90 to 5000 rpm		—Manometer —Axial pressure drop
Kuzay and Scott (1973)	Newtonian, air	$e=0.0$ $D_{in}/D_o=0.56$ Inner pipe rotating up to 1800 rpm	Turbulent	—Manometer and hot-wire —Axial pressure drop, axial and tangential mean velocities
Nouri and Whitelaw (1994)	Newtonian, glycerol and 32% tetraline in turpentine Non-Newtonian, 0.2% CMC	$e=0.0$ $D_{in}/D_o=0.5$ Inner pipe rotating at 300 rpm	Laminar and turbulent	—Manometer, laser-Doppler velocimeter —Axial pressure drop, three components of mean and rms velocities and Reynolds shear stresses

Table 2 Newtonian flow properties of 31.8% mixture of tetraline in turpentine

	N=0.0 rpm		N=300 rpm	
Outer diameter (D_o, mm)	40.3		40.3	
Inner diameter (D_{in}, mm)	20.0		20.0	
Hydraulic diameter ($D_o - D_{in}$, mm)	20.3		20.3	
Volume flow rate ($\times 10^{-3}$, m^3/s)	0.69	2.06	0.69	2.06
Inner cylinder surface velocity (V_t, m/s)	0.0	0.0	0.315	0.315
Bulk velocity (U_b, m/s)	0.72	2.14	0.72	2.14
Bulk Reynolds number (Re, $\times 10^3$)	9.0	26.6	9.0	26.6
Reynolds number of rotation (Re$_\omega$, $\times 10^3$)	0.0	0.0	1.93	1.93
Rossby number (Rs)	0.0	0.0	4.6	13.8
Mixture temperature (°C)			25.0 ± 0.02	
Density of the mixture (ρ, kg/m^3)			896.0	
Kinematic viscosity of the mixture (ν, $\times 10^{-6}$ m^2/s)			1.63	
Refractive index of the mixture at λ=589.6 nm			1.489	

encoder, which provided a train of 2000 pulses per revolution. The maximum variation in the rotational speed of the inner cylinder did not exceed ±1.5 rpm, which is equivalent to 0.5% of the inner cylinder periphery velocity $V_t = 0.315$ m/s and the amplitude of cylinder oscillation was measured to be less than ±0.15 mm, which is 1 and 3% of the widest and narrowest gaps, respectively. The bulk flow conditions and properties of the Newtonian and non-Newtonian fluids are given in Tables 2 and 3.

The effective viscosities of Table 3 were used in the calculation of effective Reynolds numbers of the non-Newtonian fluid and were obtained by determining the average wall shear stress from pressure measurements and dividing by the shear rate determined from Equation 3. Static pressures were measured with holes of 0.5-mm diameter distributed longitudinally and circumferentially in the outer diameter and connected to a calibrated manometer bank. The maximum uncertainties in manometer reading were ±5% at the lowest measured Reynolds number and considerably less at the higher Reynolds numbers.

The laser-Doppler velocimeter (LDV) was identical to that described by Nouri et al. (1993) with the principal characteristics of the optical system given in Table 4. The signal from the photomultiplier was processed by a frequency counter interfaced to a microprocessor and led to ensemble-averaged values of mean and rms velocities. The Reynolds shear stresses were obtained from rms velocity measurements in planes at ±45° to the main flow, as suggested by Melling and Whitelaw (1976). A detailed discussion on the uncertainties associated with the velocity measurements and their correction is given by Nouri et al. (1993) and is not repeated here. In brief, the maximum uncertainties in mean and rms values with the 0.2% CMC were 2.5 and 6%, respectively, after applying corrections for velocity gradient broadening.

Results and discussion

The results are presented in two subsections dealing with rotating Newtonian and non-Newtonian fluids. All velocity results have been normalized with bulk velocities U_b, and the distances are normalized with the gap between the outer to inner walls S, which varied from 5.3 to 15 mm, and that the radial distance r_1 increases inwards from outer to inner walls.

Rotating flow with Newtonian fluid

Figure 2 presents results with and without rotation at a bulk Reynolds number of 9000 and a Rossby number of 4.6; note that the direction of rotation is counterclockwise, as shown in Figure 1b. The axial mean velocities at planes 2 and 3, Figure 2a, are smaller with rotation and become larger in planes 4 and 1 with differences in the maximum velocities of the rotating and nonrotating flows in quadrants 1 to 4 of +20, −11, −14, and +9%. Also, the difference in maximum velocity between the narrowest and widest gaps, planes 1 and 3, was 21%, with rotation compared to 45% without rotation. The distortion of velocity profiles with rotation is evident and the locations of maximum velocities are not coincident with the gap center, particularly in planes 2 and 4, where they are closer to the inner and outer walls, respectively. It is also evident that the axial velocities with rotation are less than those of the stationary flow between planes 2 and 3 and greater between planes 4 and 1; the two flows

Table 3 Non-Newtonian flow properties and properties of 0.2% aqueous solution of CMC

	N=0.0 rpm		N=300 rpm	
Volume flow rate ($\times 10^{-3}$, m^3/s)	0.54	2.61	0.52	2.61
Inner cylinder surface velocity (V_t, m/s)	0.0	0.0	0.315	0.315
Bulk velocity (U_b, m/s)	0.56	2.76	0.54	2.72
Effective viscosity at wall (μ_W, $\times 10^{-3}$ kg/m·s)	10.0	6.0	9.5	6.0
Effective Reynolds number (Re, $\times 10^3$)	1.14	9.3	1.15	9.2
Reynolds number of rotation (Re$_\omega$, $\times 10^3$)	0.0	0.0	0.34	0.53
Rossby number (Rs)	0.0	0.0	3.4	17.35
CMC temperature (°C)			25.0 ± 0.02	
Density of the CMC (ρ, kg/m^3)			1000.0	
Refractive index of CMC at λ=589.6 nm			1.334	

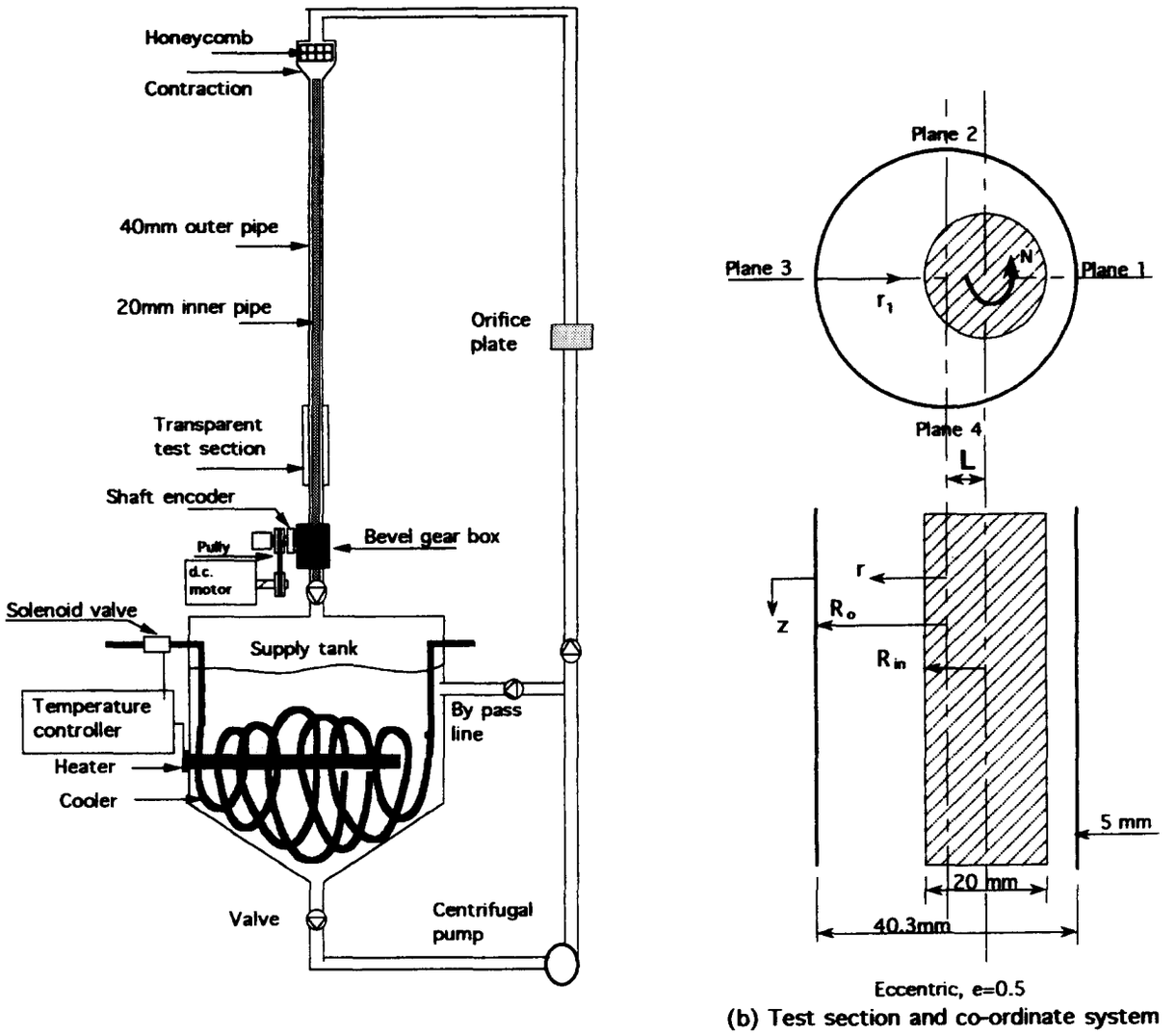

(a) Flow circuit

(b) Test section and co-ordinate system

Figure 1 Flow configuration and the coordinate system

became the same somewhere between planes 1–2 and planes 3–4.

The radial mean velocities, with negative values towards the outer pipe center, are up to 2% of the bulk velocity in planes 1 and 3, and similar to those of nonrotating flow but increase to $0.12U_b$ in plane 2 close to the inner wall, which explains the shift of the maximum axial velocity in this plane towards the inner wall. The swirl velocity profiles in planes 1 to 3 have a trend similar to that of the concentric-annulus flows of Nouri and Whitelaw (1994) and Escudier and Gouldson (1995), with a rapid decrease in tangential velocities from the inner wall to form layers close to it with thicknesses, which vary from $0.31S$ to $0.21S$ in planes 1 to 3, respectively, and near uniform in the bulk region; i.e., $0.2 < r_1/S < 0.75$. It is also evident that the penetration of the swirl velocity into the bulk flow from the inner rotating wall is reduced with increase in the gap between the two

Table 4 Characteristics of optical arrangement

Focal length of the focusing lens (mm)	300.0
Half angle of the beam interaction (deg)	5.98
Fringe spacing (μm)	3.04
Number of fringes without frequency shift	20
Diameter of the control volume at $1/e^2$ intensity in air (μm)	61.0
Length of the control volume at $1/e^2$ intensity in air (μm)	580.0
Maximum frequency shift (MHz)	±3.0
Frequency to velocity conversion (ms^{-1}/MHz)	3.04

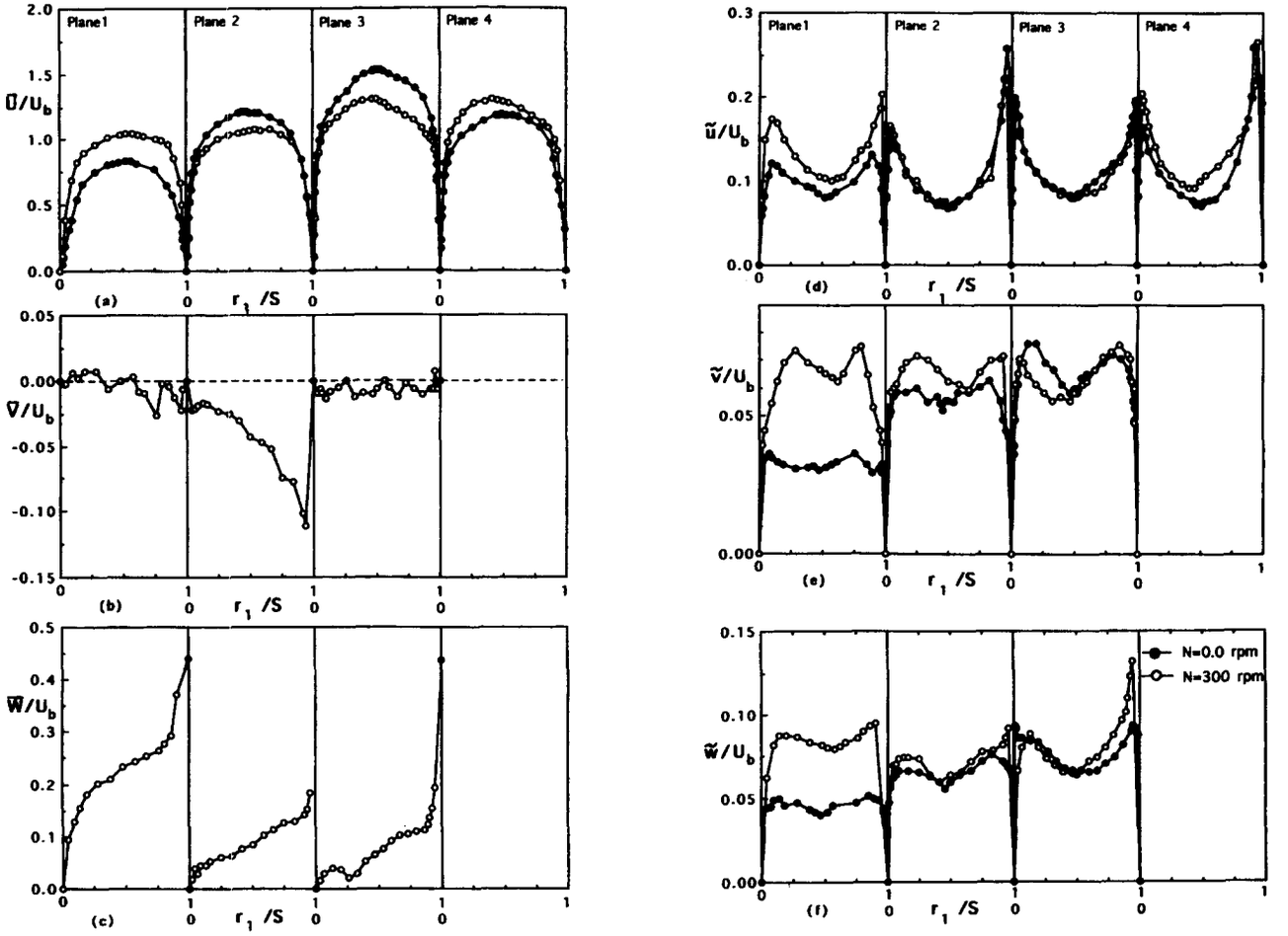

Figure 2 Rotating and nonrotating flow velocities of the Newtonian fluid at different circumferential planes for Reynolds and Rossby numbers of 9000 and 4.6: (a) axial mean velocity; (b) radial mean velocity; (c) tangential mean velocity; (d) axial rms velocity; (e) radial rms velocity; and (f) tangential rms velocity

cylinders so that there is a strong swirl in the narrow gap with values of order $0.3U_b$ and $0.15U_b$ close to the inner and outer walls, respectively. This variation of swirl velocity with gap width is opposite to that of the axial mean velocity, which increased with the gap, and suggests that the local Rossby number varies with the lowest value in the narrowest gap.

The axial rms velocities are similar with and without rotation in planes 2 and 3 but higher by up to 30% with rotation in planes 1 and 4, where the axial mean velocities became larger with stronger velocity gradient. The cross-flow turbulence intensities show small increases with rotation in planes 2 and 3 except close to the inner wall, where the differences are larger by up to 26% for the tangential component. In plane 1, the radial and tangential rms velocities with rotation, like the axial component, are higher than the nonrotating values by a factor of two. As was shown for the flow without rotation (Nouri et al. 1993), the turbulence fluctuations of all components increased with the gap to a maximum level in plane 3 (the widest), and the present results show that the differences are reduced as a consequence of rotation of the inner cylinder making the distribution of turbulence across the annulus more uniform.

Measurements of velocity characteristics with rotation at a Reynolds number of 26,600 and a Rossby number of 13.8, Figure 3, show differences in the maximum velocities between rotating and nonrotating flows of +17, −8, −6, and +7% in planes 1–4, respectively, and the difference in maximum velocity between the narrowest and widest gap is 22%, as compared to 40% without rotation. The distortion in axial mean velocity profiles with rotation is smaller than at the lower Rossby number, as might be expected, because the bulk axial flow is much stronger, so that the locations of maximum velocities are close to the gap center. The radial and tangential mean velocities of Figure 3 are similar to those at the lower Rossby number but with smaller normalized values of the order of the bulk velocity differences. The radial velocities are greatest in planes 2 and 4 with similar maximum values of $0.046U_b$ close to the inner wall but with different sign suggesting radial transports towards the inner and outer walls, respectively. The increased penetration of swirl into the bulk flow with reduction in the gap is also evident with the largest velocities in the narrow gap, where they vary from a maximum value of $0.1U_b$, close to the inner wall, to a value of $0.046U_b$ close to the outer wall.

The turbulence intensities of Figure 3 are less affected by rotation than those at the lower Reynolds number and have higher rms values with rotation in plane 1 and lower tangential rms values by about 16% in planes 2 and 3 close to the center of the gap; rotation has caused the turbulence intensities to become more uniform across the annulus. The variation of $\overline{uv}/U_b^2$ is linear across the annular gap, and the values are larger with rotation, particularly in plane 1, where the maximum values close to the inner and outer walls are higher by 39 and 50%, respectively, indicating an enhancement of the radial diffusion with

rotation, which is consistent with the increase in turbulent fluctuations. This feature of the flow is useful in drilling, because it helps to prevent accumulation of the cuttings. The results also show that the locations of zero $\overline{uv}/U_b^2$ are close to those of the maximum axial velocities and with the center of the gap, except in plane 1, where they are closer to the inner wall.

The overall average skin-friction coefficient was obtained from axial pressure measurements as

$$C_f = -\left(\frac{\partial P}{\partial z}\right)\left[\frac{d_h}{2\rho U_b^2}\right] \tag{4}$$

for Reynolds numbers from 6000 to 33,000, and Figure 4 shows a 32% higher value with rotation at the lowest Reynolds number in contrast to 3% at the highest. In the concentric-annulus of Nouri and Whitelaw (1994) and over the same range of Reynolds numbers, similar variations occurred, and there was no effect of

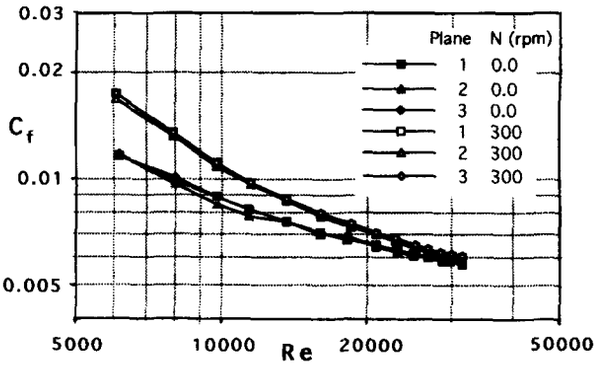

Figure 4 Skin friction coefficient of the Newtonian fluid at different circumferential planes as a function of Reynolds number

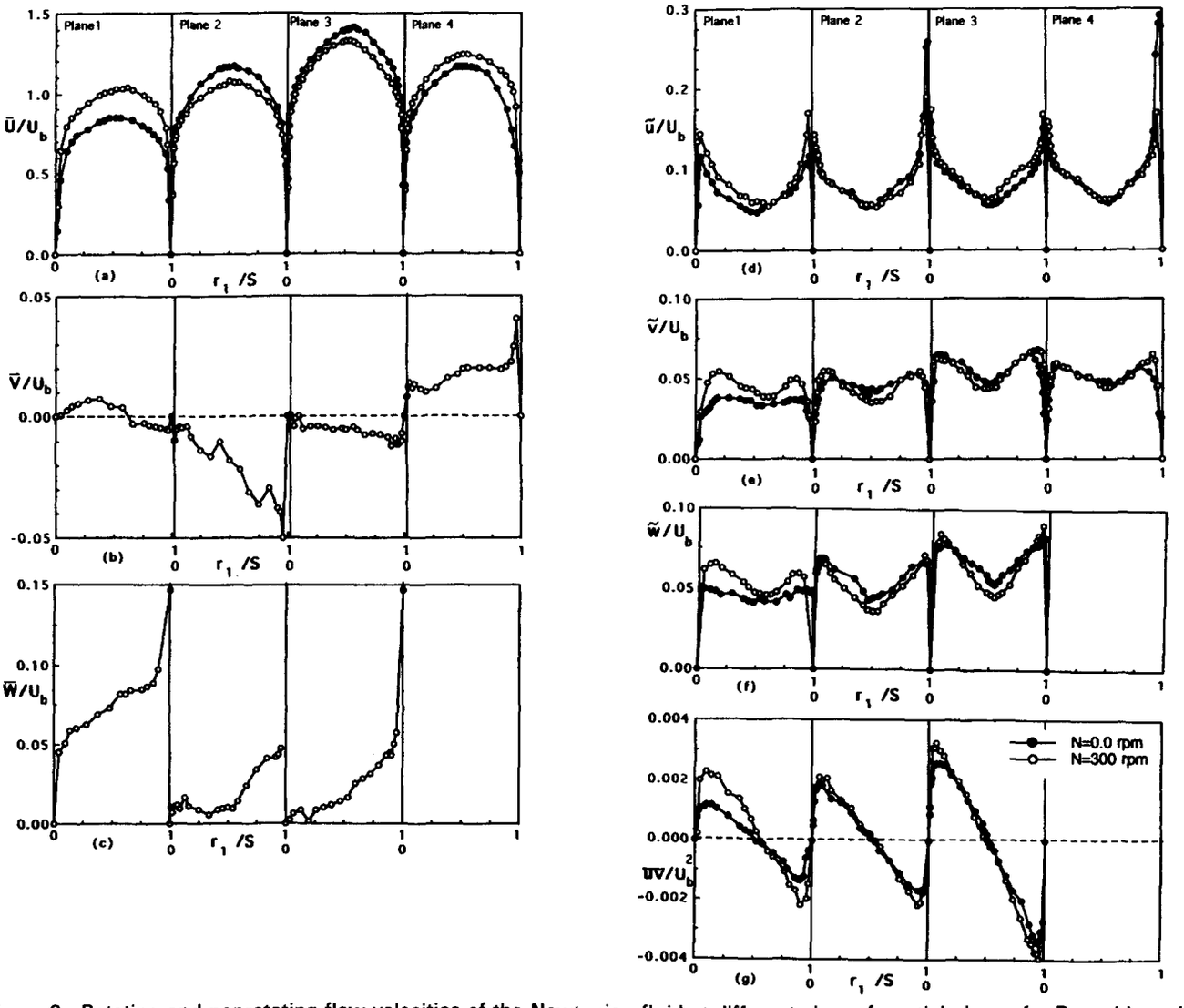

Figure 3 Rotating and nonrotating flow velocities of the Newtonian fluid at different circumferential planes for Reynolds and Rossby numbers of 26,600 and 13.8: (a) axial mean velocity; (b) radial mean velocity; (c) tangential mean velocity; (d) axial rms velocity, (e) radial rms velocity; (f) tangential rms velocity; and (e) $\overline{uv}$ cross correlation

rotation at Reynolds and Rossby numbers higher than 18,000 and 9.1, respectively. The static pressures measured on the outer cylinder in the four radial planes were identical which implies no circumferential variations in C_f.

The secondary flow circulation of Figure 5 has values up to 14.5% of the bulk velocity close to the inner wall, which is an order of magnitude greater than those detected with nonrotating flow, where there was a small secondary flow from the widest towards the narrowest gap. The circulation with rotation shows that the flow decelerated with increasing gap, and that the velocity vector decreased rapidly with distance from the inner cylinder with a tendency for a small circulation cell to be formed in the region $\pm 15°$ around plane 2 and close to the outer pipe. Only half of the flow is presented here, and no velocity measurements were made with rotation in the second half, because the laser beams would have had to pass through the rotating inner cylinder.

Rotating flow with non-Newtonian fluid

The mean velocities of the 0.2% CMC solution with rotation at effective Reynolds and Rossby numbers of 1150 and 3.4 are presented in Figure 6 together with the axial results of nonrotating flow. No measurements were made in plane 4 due to the large deflection of the light beam by the inner cylinder surface. Rotation had similar effects on the axial flow to those with Newtonian fluids with differences in maximum velocities in planes 1 to 3 between the rotating and non-rotating flows of $+28$, -23, -16% and more uniform profiles, which reduced the difference in maximum velocities between the narrowest and widest gap from 60.5% without rotation to 33% with rotation. The distortion in axial mean velocity profiles with rotation is evident, particularly, in plane 3, where the maximum velocity is shifted towards the outer wall, and in plane 2, where the axial profile is flat in the core region. The radial mean velocities in planes 1 and 3 (Figure 6b) are small with maximum values of $0.04U_b$ and $0.02U_b$, respectively, and are larger in plane 2 with a maximum value of $0.12U_b$; there is a change in radial flow direction at $r_1 = 0.35S$ below and above which the flow was towards the outer and inner

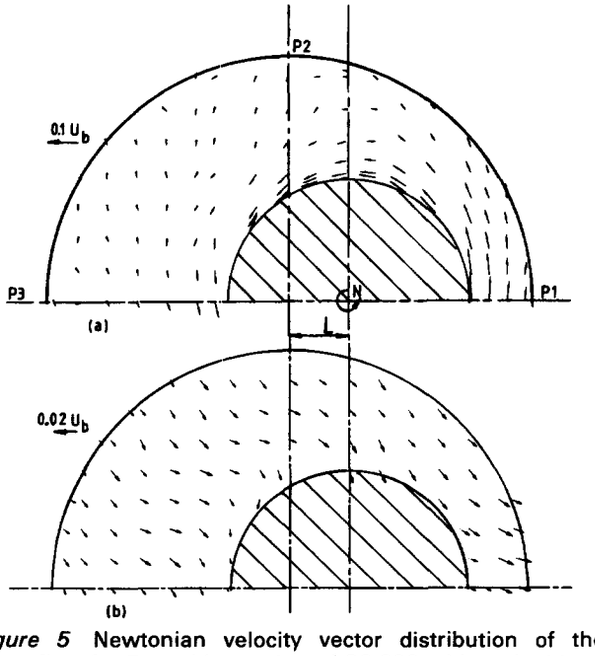

Figure 5 Newtonian velocity vector distribution of the cross-flow for Reynolds number of 26,600 with and without rotation: (a) $N = 300$ rpm; (b) $N = 0.0$ rpm

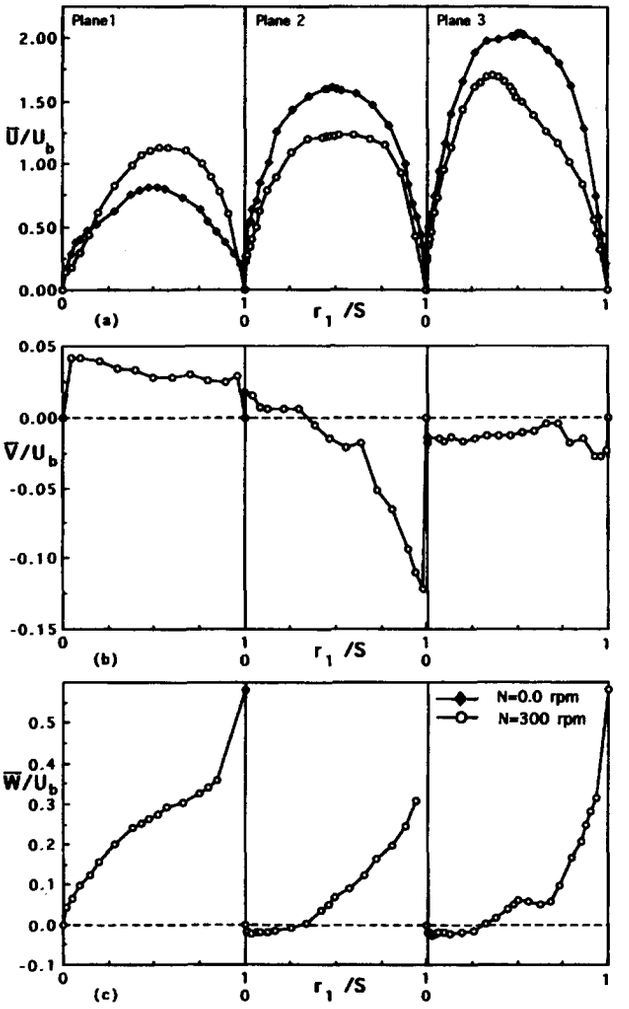

Figure 6 Rotating and nonrotating flow velocities of the 0.2% solution at different circumferential planes for Reynolds and Rossby numbers of 1150 and 3.40: (a) axial mean velocity; (b) radial mean velocity; and (c) tangential mean velocity

wall, respectively. The swirl velocities show a counter-rotating flow along the outer pipe in planes 2 and 3 with a width of about 0.33S, caused by the radial adverse pressure gradient; they suggest separation from the outer pipe between planes 1 and 2 and reattachment between planes 4 and 1.

At the Reynolds number of 9200 and Rossby number of 17.35 (Figure 7) differences from those without rotation are again evident but smaller than those of the smaller Rossby number, because the inertia of axial flow was greater and prevented the penetration of the swirl into the bulk region of the annulus; thus, reducing the effect of rotation. The distortion in the axial mean velocity profiles at the lower Rossby number is no longer evident, with locations of maximum velocities close to gap centers; the differences in maximum velocities in planes 1, 2, and 3 between the rotating and nonrotating flows are $+9$, -11, -7.7%. The radial velocities are half those at the lower Rossby number, and the tangential velocity profiles of Figure 7c show, as with the Newtonian fluid, a rapid decay in the vicinity of the inner wall and a much slower decay in the core region with the larger values in the narrowest gap: there is no counter-rotation at this Rossby number.

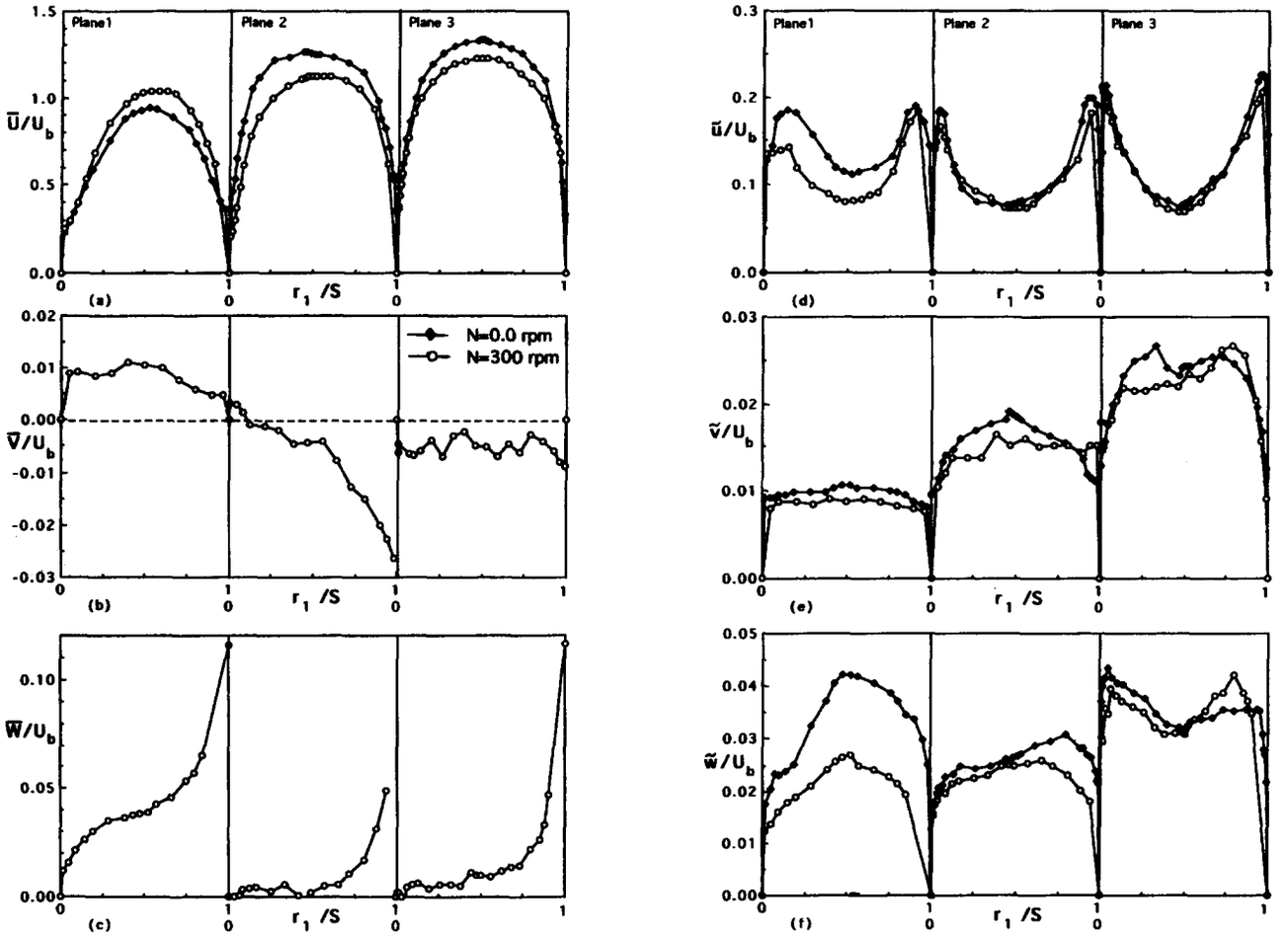

Figure 7 Rotating and nonrotating flow velocities of the 0.2% solution at different circumferential planes for Reynolds and Rossby numbers of 9200 and 17.35: (a) axial mean velocity; (b) radial mean velocity; (c) tangential mean velocity; (d) axial rms velocity; (e) radial rms velocity; and (f) tangential rms velocity

Table 5 summarizes the local Rossby numbers defined in terms of the maximum axial velocities in each gap and the tip velocity of the inner cylinder, as $Rs_m = 2U_m/\omega R_{in}$, and shows that it increases with the gap and that this variation is less with 0.2% CMC solution. The maximum difference occurs between planes 1 and 3, and the value with the 0.2% CMC solution is 10.5% less than that with the Newtonian fluid for the same Reynolds number.

The turbulence intensities of Figures 7d to f are similar to those without rotation for all three components in planes 2 and 3, but the axial and tangential components in the narrowest gap were reduced by rotation by up to 28 and 40%, respectively,

Table 5 Circumferential variation of Rossby number

	(a) Tetraline/turpentine mixture				
	Plane 1	Plane 2	Plane 3	Plane 4	$Rs_{m,1}/Rs_{m,3}$
Local Rossby number Rs_m, at Re=9000	4.76	5.0	6.25	5.70	0.76
Local Rossby number Rs_m, at Re=26,600	14.08	14.7	18.2	16.9	0.77
(b) 0.2% Aqueous solution of CMC					
	Plane 1	Plane 2	Plane 3		$Rs_{m,1}/Rs_{m,3}$
Local Rossby number Rs_m, at Re=1150	3.85	4.25	5.88		0.655
Local Rossby number Rs_m, at Re=9200	17.86	19.42	21.05		0.85

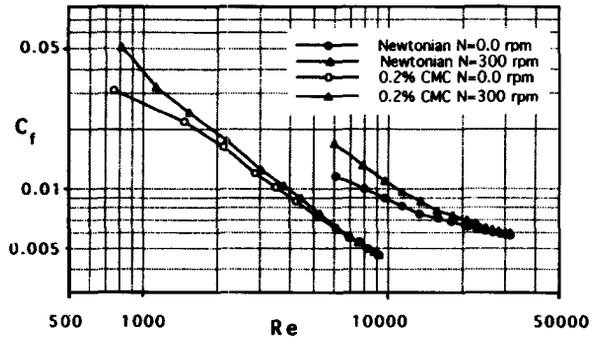

Figure 8 Skin friction coefficient of the Newtonian and non-Newtonian fluids as a function of Reynolds number

which is opposite to that observed with the Newtonian fluids for a similar Reynolds number. The reason may be that the nonrotating flow in the narrow gap with the Newtonian fluid is more turbulent than with the 0.2% CMC solution for a similar Reynolds number as shown in Nouri et al. (1993).

Variations of the average skin friction coefficient with Reynolds number are shown in Figure 8. Without rotation, the variation of C_f with the 0.2% CMC solution is similar to that of Nouri et al. (1993), with an extended range of nonturbulent flow and drag reduction of 50% at the highest Reynolds number of 9200 (defined as $d_r = 100 \times [(C_{f_n} - C_{f_p})/C_{f_n}]$ where suffixes n and p represent the skin-friction coefficient for Newtonian and non-Newtonian fluids). In the laminar region, the values of C_f with rotation are higher by 38% at the lowest measured Reynolds number and similar at 6100. The drag reduction with rotation is about 61%, which is higher than without rotation. The results in laminar flow do not show a uniform increase of flow resistance with rotation, as they did with the concentric annulus, but are uniformly higher than the analytical solution for the Newtonian fluid ($C_f = 17.8\ \mathrm{Re}^{-1}$; Shah and London 1978) up to a Reynolds number of 5000.

Figure 9 allows comparison of mean swirl velocities with the two fluids. The swirl velocity increased as the Rossby or Reynolds number decreased, as might be expected, because the inertia effect became less. The penetration of the swirl velocities also increased with decrease in the gap due to the corresponding reduction in local Rossby number so that they were largest in the narrow gap, where the swirl velocities of the Newtonian and non-Newtonian fluids tended to become similar when their Rossby numbers were close.

At the Reynolds number of 9200 with rotation, the axial rms variations of Figure 10 are similar, except in plane 1, where the

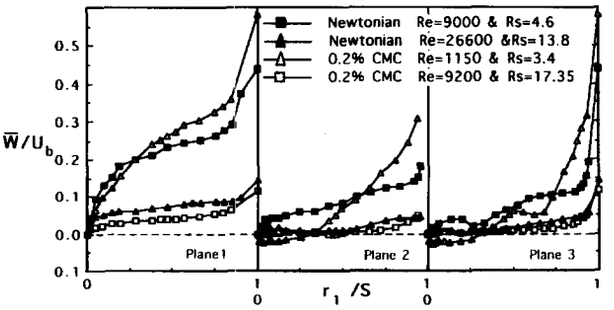

Figure 9 Comparison of the swirl velocity of the Newtonian and non-Newtonian fluids at an inner cylinder rotational speed of 300 rpm

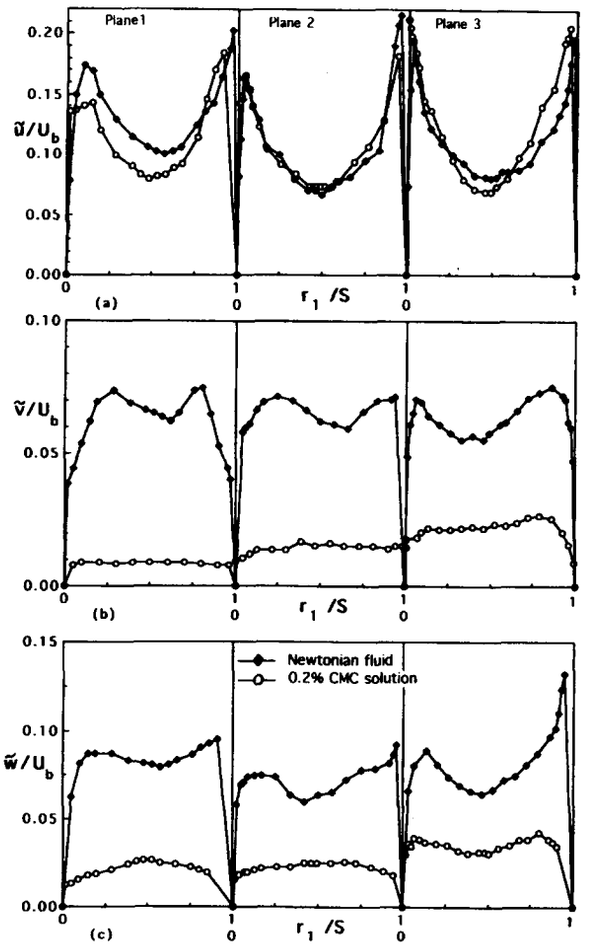

Figure 10 Comparison of the Newtonian and non-Newtonian fluid flows with Reynolds number of 9200 and an inner cylinder rotational speed of 300 rpm: (a) axial rms velocity; (b) radial rms velocity; and (c) tangential rms velocity

0.2% CMC fluid led to values lower by around 21%. The cross-flow velocity fluctuations with the CMC solution were suppressed in all planes and more so as the gap was reduced, so that the CMC radial and tangential rms values at the center of the widest gap were 2.1 and 2.6 times lower than the Newtonian values, respectively, and these factors increased to 6.9 and 4.6 in plane 1. Similar effects were present with the nonrotating flows but to a lesser extent, consistent with the lower drag reduction. This suppression of turbulence intensities was due to the molecular stretching of the polymer solution, which is consistent with all previous experimental investigation in duct flows. The reason for the larger differences in the turbulence intensities with rotation is the lower Rossby number (or inertia) of the Newtonian fluid, which makes the penetration of the swirl velocity into the bulk flow easier and more effective so that the overall increase in cross-flow turbulence intensities with the Newtonian fluid was greater.

Conclusions

The results of this paper add to those of Nouri et al. (1993), where the flows of Newtonian and non-Newtonian fluids in a concentric and two eccentric annuli were examined without

rotation of the inner cylinder. The more important effects of rotation are as follows:

(1) In general, rotation caused the distributions of the mean and rms of the axial velocities across the annulus to become more uniform with large variations in cross-flow mean velocities; this effect diminished as the bulk velocity or Rossby number increased. The radial distribution of the tangential mean velocity decayed rapidly close to the inner wall, with a more uniform profile in the core region with levels which decreased with Rossby number. The angular distributions showed maximum values in the narrowest gap. The swirl velocities with both fluids were similar when the Rossby numbers of both flows were similar. With the Newtonian fluid and Rossby and Reynolds numbers of 13.8 and 26,600, respectively, the secondary flow velocity vectors showed a circulation in the direction of rotation with values up to 14% of the bulk velocity close to the inner wall in the narrow gap.

(2) With the Newtonian fluid, rotation had little effect on turbulence intensities in planes 2 and 3 of Figure 1, but considerable increases in the rms of the three velocity components occurred in the plane of the narrowest gap. With the polymer solution, rotation caused a reduction in the rms of the three velocity components in the narrow gap.

(3) The flow resistance with Newtonian and non-Newtonian fluids increased by more than 30% with rotation at the lowest Reynolds number and was almost unaffected at the highest Reynolds numbers. The extension of the nonturbulent flow region with the CMC solution was evident, with drag reduction of the order of 61% at a Reynolds number of 9200, consistent with suppression of large turbulence intensities.

(4) With the polymer solution in laminar flow, rotation caused a counter-rotating swirl flow along the outer pipe wall with a width of about 0.33 times the local radial distance between the two cylinders. This counter-rotating flow was absent at the higher Reynolds and Rossby numbers of 9200 and 17.35.

Acknowledgments

Financial support from the British Petroleum PLC is gratefully acknowledged.

References

Brighton, J. A. and Jones, J. B. 1964. Fully developed turbulent flow in annuli. *J. Basic Eng.*, **86**, 835–844

Escudier, M. P., Gouldson, I. W. and Jones, D. M. 1994. Flow of shear-thinning fluids in a concentric annulus. *Exp. Fluids*, **18**, 1–14

Escudier, M. P. and Gouldson, I. W. 1995. Concentric annular flow of shear thinning liquids with centerbody rotation. *Int. J. Heat Fluid Flow*, **16**, 156–162

Jonsson, V. K. and Sparrow, E. M. 1966. Experiments on turbulent flow phenomena in eccentric annular ducts. *J. Fluid Mech.*, **25**, 65–85

Kacker, S. C. 1973. Some aspects of fully developed turbulent flow in non-circular ducts. *J. Fluid Mech.*, **57**, 583–602

Kuzay, T. M. and Scott, C. J. 1973. Turbulent heat and momentum transfer studies in an annulus with rotating inner cylinder. University of Minnesota, Heat Transfer Laboratory, TR 111

Lawn, C. J. and Elliott, C. J. 1972. Fully developed turbulent flow through concentric annuli. *J. Mech. Eng. Sci.*, **14**, 195–204

Melling, A. and Whitelaw, J. H. 1976. Turbulent flow in a rectangular duct. *J. Fluid Mech.*, **78**, 289–315

Nouri, J. M. and Whitelaw, J. H. 1994. Flow of Newtonian and non-Newtonian fluids in a concentric annulus with rotation of the inner cylinder. *J. Fluid Eng.*, **116**, 821–827

Nouri, J. M., Umur, H. and Whitelaw, J. H. 1993. Flow of Newtonian and non-Newtonian fluids in concentric and eccentric annuli. *J. Fluid Mech.*, **253**, 617–641

Nouri, J. M. and Whitelaw, J. H. 1990. Flow characteristics of stirred reactors with Newtonian and non-Newtonian fluids. *AIChE J.*, **36**, 627–629

Nouri, J. M., Whitelaw, J. H. and Yianneskis, M. 1988. A refractive index matching technique for solid/liquid flows. *Laser Anemometry Fluid Mech.*, **3**, 335–346

Pinho, F. T. and Whitelaw, J. H. 1990. Flow of non-Newtonian fluids in a pipe. *J. Non-Newtonian Fluid Mech.*, **34**, 129–144

Pinho, F. T. and Whitelaw, J. H. 1991. The flow of non-Newtonian fluids over a confined baffle. *J. Fluid Mech.*, **226**, 475–496

Quarmby, A. 1967. An experimental study of turbulent flow in concentric annuli. *Int. J. Mech. Sci.*, **9**, 205–221

Rehme, K. 1974. Turbulent flow in smooth concentric annuli with small radius ratios. *J. Fluid Mech.*, **64**, 263–287

Shah, R. K. and London, A. L. 1978. *Laminar flow forced convection in ducts.* Academic Press, New York

Yamada, Y. 1962. Resistance of a flow through an annulus with an inner rotating cylinder. *Bull. JSME*, **5**, 302–310